Intracellular Mechanochemical Waves in an Active Poroelastic Model

Markus Radszuweit,[1,2] Sergio Alonso,[1] Harald Engel,[2] and Markus Bär[1]

[1]*Physikalisch-Technische Bundesanstalt, Abbestrasse 2-12, 10587 Berlin, Germany*

[2]*Institute for Theoretical Physics, Technische Universität Berlin, Hardenbergstrasse 36, 10623 Berlin, Germany*

(Received 22 June 2012; published 25 March 2013)

Many processes in living cells are controlled by biochemical substances regulating active stresses. The cytoplasm is an active material with both viscoelastic and liquid properties. We incorporate the active stress into a two-phase model of the cytoplasm which accounts for the spatiotemporal dynamics of the cytoskeleton and the cytosol. The cytoskeleton is described as a solid matrix that together with the cytosol as an interstitial fluid constitutes a poroelastic material. We find different forms of mechanochemical waves including traveling, standing, and rotating waves by employing linear stability analysis and numerical simulations in one and two spatial dimensions.

DOI: 10.1103/PhysRevLett.110.138102 PACS numbers: 87.17.Aa, 82.40.Bj, 87.16.Ln, 87.16.Uv

Introduction.—Studying the spatiotemporal instabilities and the related symmetry breaking has become a relevant tool to understand many biological processes. In his pioneering work [1], Turing suggested the interplay of reactions and diffusion processes as a mechanism for morphogenesis. Later, an alternative mechanochemical approach was developed that emphasizes the role of forces and deformations in tissue morphogenesis [2]. Recently, the reaction-diffusion mechanism proposed by Turing was applied to pattern formation in single cells and shown to be relevant, e.g., for cell polarity [3] and the control of cell division [4]. Analogous to the earlier work on tissues, models for intracellular pattern formation have recently been derived that include mechanical forces and the resulting advection processes [5,6].

Many processes such as cell movement [7] and cell division [8] are connected with a transport of cytoplasm. Transport in cells does not only occur by passive diffusion [9]; it can be driven by stress generation from cytoskeletal filaments [10,11]. The cytoskeleton is an active cellular material in the form of a network of filaments [12]. Molecular motors control the mechanical properties of this network and keep the system far from thermodynamic equilibrium. Active gel models describe the cytoskeleton as a viscous fluid [13] and were used to describe cortical flows in polarized cells [5,14] as well as aspects of cell motility [15].

In contrast, experiments on inhomogeneous hydration in cells, where large pressure gradients in the cell are observed [16], indicate that the cytoplasm can behave like a porous elastic spongelike solid (cytoskeleton) penetrated by a viscous fluid phase (cytosol) [17]. Moreover, multiphase flow models have been proposed as appropriate description of cytoplasmic dynamics [18].

In this Letter, we derive and investigate a generic poroelastic two-phase model of the cytoplasm assuming a viscoelastic solid phase and a fluid phase. Furthermore, we incorporate an active tension in the solid phase which depends on the concentration of a regulating agent that is advected by the fluid phase. This model may be extended to describe diverse cellular phenomena happening at sufficiently short time scales, e.g., local deformations on protoplasmic droplets of *Physarum polycephalum* [19] or fiber contraction of muscle cells [20]. For these examples, the temporal period of oscillations and waves is smaller than the characteristic time at which the cytoskeleton exhibits fluid behavior. The resulting equations describe the cytoskeleton as an active viscoelastic solid coupled to a passive fluid in contrast to earlier works that model the cytoskeleton itself as an active fluid [5], which was derived to account for cellular processes at long time scales, where fluidization of the cytoskeleton occurs. We show that the interplay of active tension, fluid flow, and the mechanical force balance with mass conservation is sufficient to induce mechanochemical waves in the active poroelastic medium. In contrast to other models for intracellular wave formation, no chemical reaction kinetics is required in this model.

Model.—We assume that the cell cytoplasm is formed by two phases [7], a viscoelastic solid phase and a fluid phase corresponding to the cytoskeleton and the cytosol, respectively; see Fig. 1(a). The total stress in the cytoplasm is the sum of two contributions: $\sigma = \rho_s \sigma_s + \rho_f \sigma_f$, where σ_s and σ_f are the viscoelastic solid and fluid stresses, respectively. The quantities ρ_f and ρ_s describe the fluid and solid volume fractions, respectively. They satisfy $\rho_f + \rho_s = 1$ and are assumed to be constant.

Depending on the stress, cells can exhibit fluid or solid properties [21]. Therefore, one has to take into account viscoelasticity. Two classical models have typically been used to study cell viscoelasticity, the Maxwell model and the Voigt model [22]. Whereas the cytoskeleton has been described as an active gel by employing the Maxwell model earlier [15,23], here we follow the alternative approach that assumes that the cytoskeleton is a viscoelastic solid described by the Voigt model [24–27]. We derive

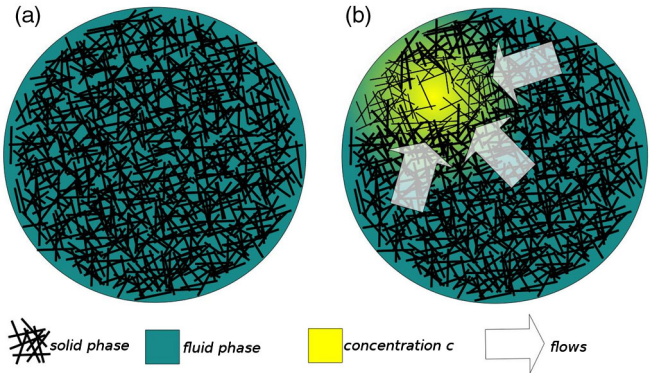

FIG. 1 (color online). (a) Cytoplasm is formed by two phases, a solid and a fluid phase. (b) Sketch of the inhomogeneous stress generation. A local increase in the concentration deforms the viscoelastic solid phase and induces convection of the fluid and of the component c which regulates the stress. The arrows indicate the flow direction.

the active poroelastic model in one spatial dimension; for the extension to 2D, see [28]. According to the Voigt model, the stress in the solid phase is given by

$$\sigma_s = E\partial_x u + \eta_s \partial_x \dot{u} + T, \tag{1}$$

where E is the Young modulus and η_s the viscous damping coefficient of the cytoskeleton. We assume that the cytoskeleton forms an elastic solid network, and u is the local shift field that describes the material's deformation. Equation (1) is based on linear elasticity and is valid for small strain ($|\partial_x u| \ll 1$). Finally, Eq. (1) contains a term describing an active tension $T(c)$, which depends on the concentration c of an advected regulating chemical agent in the fluid phase. The viscous stress in the fluid phase is given by

$$\sigma_f = \eta_f \partial_x v, \tag{2}$$

where v is the velocity field and η_f the viscosity of the cytosol. The incompressibility condition [7] for the poroelastic system reads

$$\partial_x(\rho_f v + \rho_s \dot{u}) = 0. \tag{3}$$

It describes the deformation of the solid phase by the flow and the generation of flows by deformations of the solid phase. We neglect changes on ρ_f and ρ_s, assuming small strain and small displacement u (for a detailed argument, see [28]). For specific boundary conditions [29], Eq. (3) gives rise to a linear dependence of the rate of deformation on the fluid velocity $\dot{u} = -v\rho_f/\rho_s$. The force balance is expressed as

$$\rho_s \partial_x \sigma_s = f_s + \rho_s \partial_x p, \qquad \rho_f \partial_x \sigma_f = f_f + \rho_f \partial_x p, \tag{4}$$

where p is an additional pressure stemming from the incompressibility condition [7]. Additional osmotic pressures are neglected. Using Darcy's law for porous media, one obtains the drag force terms as

$$f_f = -f_s = \rho_f \rho_s \beta (v - \dot{u}), \tag{5}$$

where the parameter β is the ratio between the dynamic viscosity η_f and the permeability κ_0 of the fluid [30]. Instead of the fluid velocity v, we consider the velocity relative to the body reference frame $w = v - \dot{u}$. The velocities of both phases can be expressed in terms of w. One obtains $v = w\rho_s$ and

$$\partial_t u = -w\rho_f. \tag{6}$$

The pressure introduced in Eqs. (4) can be eliminated, which gives rise to

$$\eta \partial_x^2 w - E\partial_x^2 u - \partial_x T - \beta w = 0, \tag{7}$$

where the coefficient η is defined by $\eta = \rho_f \eta_s + \rho_s \eta_f$. Equations (6) and (7) describe the dynamics of the poroelastic medium. Finally, the advection and diffusion of a biochemical substance that regulates the active tension is modeled by

$$\partial_t c + \partial_x (wc) = D\partial_x^2 c, \tag{8}$$

where c is the concentration of the agent and D its diffusion coefficient. From Eq. (8), it follows that the spatial average of c is conserved:

$$\frac{1}{L}\int_0^L c dx = c_0. \tag{9}$$

Hence, c_0 is a parameter that needs to be fixed by initial conditions for a complete specification of the model. The concentration c can increase locally due to the advection of the fluid phase; see Fig. 1(b).

We choose the dependence of the local active tension as

$$T(c) = T_0 - \xi f(c) = T_0 - \xi \frac{c}{1+c}, \tag{10}$$

which assumes that a homogeneous active tension T_0 is produced, e.g., by a constant density of molecular motors in the cytoskeleton. The local active tension $T(c)$ may vary in space because it is regulated by a chemical agent with a (potentially) spatially inhomogeneous concentration $c(x)$ resulting from Eq. (8). The sign of ξ determines if the chemical regulator with concentration c activates ($\xi < 0$) or inhibits ($\xi > 0$) the active tension.

The model Eqs. (6)–(8) can be conveniently scaled by introducing a characteristic length $\ell = \sqrt{\eta/\beta}$ and a characteristic time $\tau = \ell^2/D$. The length ℓ depends on the effective viscosity which, since $\eta_f \ll \eta_s$, reduces to $\eta \approx \eta_s \rho_f$, where $\eta_s \approx 10^4$ Pa s [15]. The parameter β is the ratio of the fluid viscosity $\eta_f \approx 2 \times 10^{-2}$ Pa s [16] and the permeability $\kappa_0 \approx 0.0002\ \mu\text{m}^2$, which is the square of the characteristic pore radius (15 nm) of the solid phase of cytoplasm [16]. These estimates yield a characteristic length of $\ell \approx 7\ \mu$m. Assuming that the concentration c corresponds to calcium ions, with a diffusion coefficient $D \approx 200\ \mu\text{m}^2/\text{s}$, a characteristic time $\tau \approx 0.2$ s follows.

Linear stability analysis.—The spatially homogeneous steady state solution of Eqs. (6)–(8) is given by a constant concentration ($c = c_0$) and a motionless medium ($w = 0$ and $u = 0$). A linear stability analysis of this steady state with respect to small perturbations of the form $(\delta w, \delta u, \delta c)e^{ikx+\lambda t}$ yields the eigenvalues

$$\lambda = -\frac{1}{2}\frac{\ell^2 k^2}{\tau}\left(A \pm \sqrt{A^2 - 4\frac{M}{(1+\ell^2 k^2)}}\right), \qquad (11)$$

where we have defined the dimensionless number $A = 1 - [\mathrm{Pe} c_0 \partial_c f(c_o) - M](1+\ell^2 k^2)^{-1}$ and the Péclet number that is given by the ratio of the diffusive to advective time scales $\mathrm{Pe} = \xi/(D\beta)$, similar to the approach in [5]. Moreover, we define an additional dimensionless number $M = E\rho_f/(D\beta)$ that describes the ratio of the diffusive to elastic time scales.

Whereas for a stress activating coupling constant $\xi < 0$ the spatially homogeneous state is always linearly stable, the opposite case $\xi > 0$ (inhibitory coupling) can lead to an instability of the spatially homogeneous state. Hence, we will concentrate on this case in the remainder of the Letter. Four qualitatively different regions are observed in the parameter plane spanned by Pe and M; see Fig. 2(a). For $M = 0$ and above a critical Péclet number Pe, the system is unstable against modes with purely real eigenvalues [Fig. 2(b)], and static profiles of high concentration are seen in simulations, similar to the findings in [5]. For large enough values of M [region IV in Fig. 2(a)], the homogeneous steady state is stable. For intermediate values of M in Fig. 2(a), one finds either unstable modes with both real and imaginary eigenvalues [region II in Figs. 2(a) and 2(c)] or only unstable modes with oscillatory eigenvalues [region III in Figs. 2(a) and 2(d)]. Hence, one expects wave dynamics to emerge and not only stationary patterns. Additional numerical simulations are necessary to obtain the nonlinear dynamics of the resulting spatiotemporal patterns.

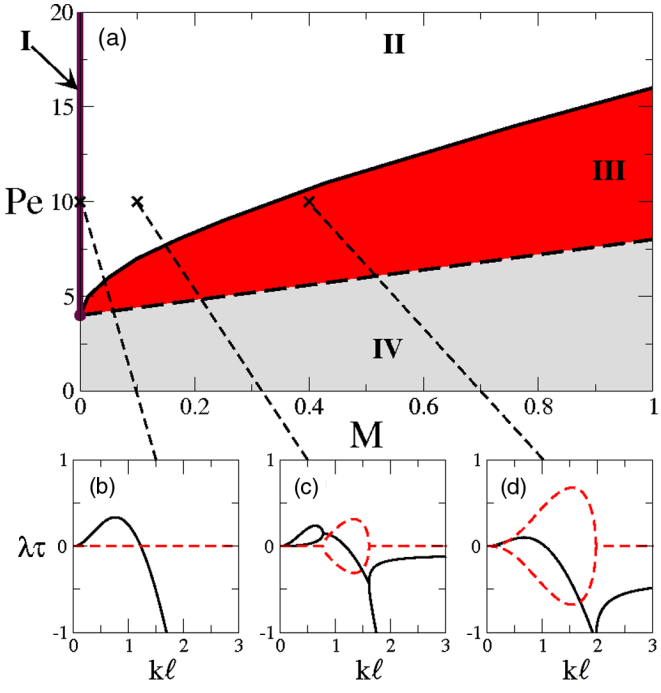

FIG. 2 (color online). (a) Phase diagram in the Pe-M plane obtained from the linear stability analysis of Eqs. (6)–(8) with $c_0 = 1$. In region I, corresponding to $E = 0$, the unstable modes are always real. In region II, the unstable modes are formed by real and complex bands. In region III, the unstable modes are complex. In region IV, all the modes are stable, with no pattern formation. Dispersion relations for values of the parameters correspond to (b) region I, (c) region II, and (d) region III. The solid and dashed lines show the real and the imaginary parts of the eigenvalues, respectively. The crosses in the phase diagram indicate the parameter values employed in (b)–(d).

Numerical simulations.—We integrate Eqs. (6)–(8) numerically in a one-dimensional domain using a finite differences method [29]. Moreover, realistic parameter values are used based on the above considerations. In Fig. 3, an example of spatiotemporal dynamics in region III of Fig. 2(a) is shown. Standing waves are observed for sufficiently large values of M. Profiles of the variables show the spatial accumulation of the concentration c and the balanced profiles of w and u. For small values of E, the deformations of the solid phase become large ($|\partial_x u| > 1$). This implies that the deformations of the medium are not captured by the linear elasticity term in Eq. (1) anymore. To avoid this difficulty, we consider the somewhat unphysiological case $\rho_f \ll 1$ [see Eq. (6)] to quantitatively explore the whole phase diagram of Fig. 2(a).

Figure 4(a) shows the resulting phase diagram obtained from systematic numerical simulations, which is in

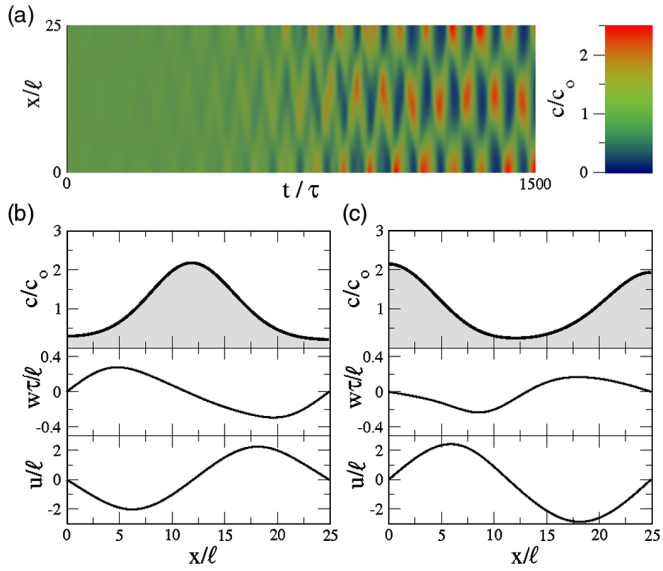

FIG. 3 (color online). (a) Spatiotemporal evolution of the concentration c. Profiles of concentration c (upper frame), velocity w (middle frame), and shift field u (lower frame) for two times (b) 1460τ and (c) 1500τ. Parameter values $\mathrm{Pe} = 10$, $M = 1.25$, $c_0 = 1$, and $\rho_f = 0.5$.

excellent agreement with the phase diagram [Fig. 2(a)] obtained from linear stability analysis. From a random initial condition, the system develops static patterns for $M = 0$; see Fig. 4(b). For nonzero values of M, traveling domains are observed that exhibit coarsening and reflection at the boundaries; see Fig. 4(c). Upon increase of M, the dynamics becomes complex and irregular; see Fig. 4(d). At even bigger values of M, standing waves similar to the ones in Fig. 4(a) are observed; see Fig. 4(e). For large values of M, the steady state is stable.

To study spatiotemporal patterns in 2D, an extension of Eqs. (6)–(8) is used [28]. The numerical simulations are performed with a finite elements method. As predicted by linear stability analysis and already observed in 1D simulations, standing waves are obtained for larger values of M; see Figs. 5(a) and 5(b). However, in two dimensions, standing waves are often only transient and are replaced by rotating waves; see Fig. 5(c).

Discussion.—Motivated by two-phase flow models of amoeboid movement, we introduce a model that combines the dynamics of a viscoelastic solid with the one of a viscous fluid. Pattern formation is investigated with linear stability analysis and numerical simulation. We find that the presence of elastic forces ($E \neq 0$) leads to the formation of mechanochemical waves. These waves occur due to the interplay of the following processes: active tension in the solid (cytoskeletal) phase, flow, and transport of a regulating chemical agent in the fluid (cytosolic) phase. Depending on the magnitude of the Young modulus E traveling domains, turbulent and standing waves are obtained. In two dimensions, the results of simulations are analogous to the 1D results, but, in addition, rotating waves are observed.

This Letter provides a description of mechanically induced transport in a model of an active poroelastic medium. The cytoplasm is described as a viscoelastic solid cytoskeleton interpenetrated by a viscous cytosol. Hence, processes of the unbinding of cross-linkers and depolymerization that may appear on large time scales are neglected [12]. Alternative descriptions in terms of active gels account for larger time scales [15]. Depending on the cell type and particular conditions, the concrete value of this time scale differs. A typical value for solid-fluid transitions in eukaryotic cells is around 5–10 s [15,21].

Hence, the poroelastic model applies to mechanochemical waves with periods shorter than the characteristic solid-fluid transition time. A potential application is the slime mold *Physarum polycephalum* that was found to have a relaxation time of several minutes under stretch [31] and

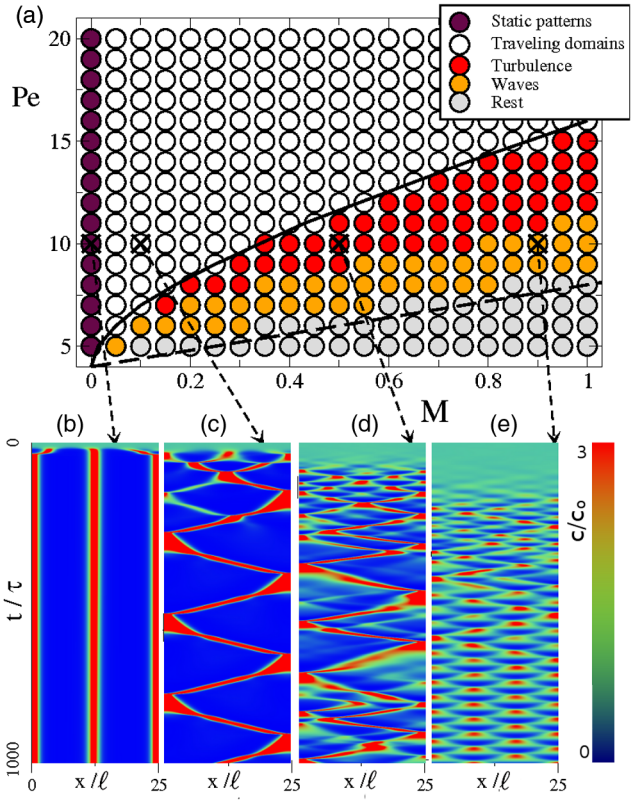

FIG. 4 (color online). (a) Phase diagram in the Pe-M plane obtained by numerical simulations of Eqs. (6)–(8) with $\rho_f = 0.01$. The lines correspond to the analytic results shown in Fig. 2. Examples of spatiotemporal plots of the concentration c in a one-dimensional medium are shown in (b) static patterns, (c) traveling domains, (d) turbulent patterns, and (e) standing waves. The crosses in the phase diagram indicate the parameter values employed in (b)–(e).

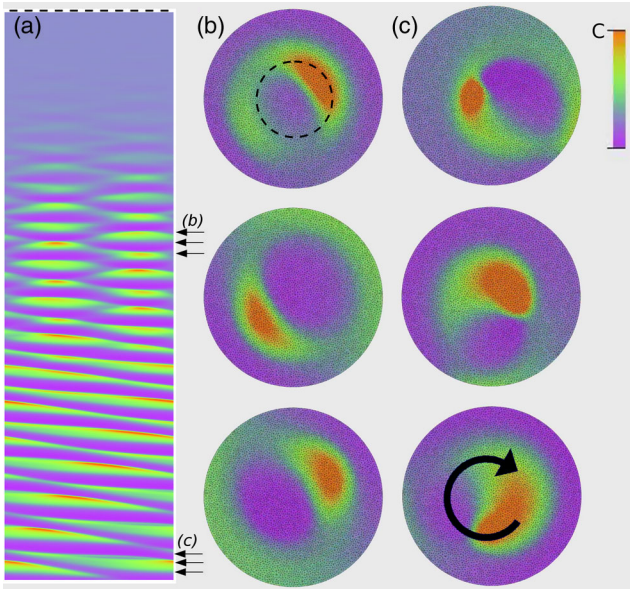

FIG. 5 (color online). Two-dimensional concentration patterns in a circular domain with diameter 25ℓ. (a) Spatiotemporal plot obtained along the dashed line indicated in the upper frame of (b). The integration time was 500τ. Two-dimensional (b) standing and (c) rotating waves. The small arrows in (a) mark the time corresponding to the snapshots in (b) and (c). The circular arrow shows the direction of rotation.

shows mechanochemical waves on time scales of 1 min [19,32,33]. Mechanochemical waves are also observed during the oscillatory contraction of the fibers of muscle cells [20] that also behave elastically during oscillations with periods of 2 s [24].

Several extensions of the presented model are possible. For the case of large deformations, one can explicitly incorporate the deformations by a stress tensor based on nonlinear elasticity. A more general model that describes the concentration dynamics of more than one biochemical species as well as chemical reactions between such species can easily be obtained by deriving coupled reaction-advection-diffusion equations. This is analogous to earlier work on the modeling of active fluids [5].

Standing, traveling, and rotating waves are found in this model if an active tension inhibiting substance is advected as a result of mechanical contractions. A candidate of such a substance is calcium that is known to decrease active tension in some cellular systems like *Physarum polycephalum* [19]. The most remarkable aspect of the poroelastic model described in this Letter is that mechanochemical waves do naturally arise even in the absence of kinetic biochemical oscillations that were assumed to be absolutely necessary to account for contraction waves in cells in earlier work [27,33].

We acknowledge financial support from the German Science Foundation DFG within SFB 910 "Control of Self-Organizing Nonlinear Systems" and GRK 1558 "Nonequilibrium Collective Dynamics in Condensed Matter and Biological Systems."

Note added in proof.—Recently, a related model for chemomechanical instabilities was suggested and analyzed, that is based on a different chemical feedback mechanism and employs a nonlinear elastic model [34].

[1] A. M. Turing, Phil. Trans. R. Soc. B **237**, 37 (1952).
[2] J. D. Murray, P. K. Maini, and R. T. Tranquillo, Phys. Rep. **171**, 59 (1988).
[3] N. W. Goehring, P. K. Trong, J. S. Bois, D. Chowdhury, E. M. Nicola, A. A. Hyman, and S. W. Grill, Science **334**, 1137 (2011).
[4] M. Loose, K. Kruse, and P. Schwille, Annu. Rev. Biophys. **40**, 315 (2011).
[5] J. S. Bois, F. Jülicher, and S. W. Grill, Phys. Rev. Lett. **106**, 028103 (2011).
[6] J. Howard, S. W. Grill, and J. S. Bois, Nat. Rev. Mol. Cell Biol. **12**, 392 (2011).
[7] W. Alt and M. Dembo, Math. Biosci. **156**, 207 (1999).
[8] G. Salbreux, J. Prost, and J. F. Joanny, Phys. Rev. Lett. **103**, 058102 (2009).
[9] T. Nakagaki and R. D. Guy, Soft Matter **4**, 57 (2007).
[10] G. F. Oster and G. M. Odell, Physica (Amsterdam) **12D**, 333 (1984).
[11] T. Betz, D. Koch, Y.-B. Lu, K. Franze, and J. A. Käs, Proc. Natl. Acad. Sci. U.S.A. **108**, 13420 (2011).
[12] F. C. MacKintosh and C. F. Schmidt, Curr. Opin. Cell Biol. **22**, 29 (2010).
[13] J. F. Joanny and J. Prost, HFSP J. **3**, 94 (2009).
[14] M. Mayer, M. Depken, J. Bois, F. Jülicher, and S. Grill, Nature (London) **467**, 617 (2010).
[15] F. Jülicher, K. Kruse, J. Prost, and J.-F. Joanny, Phys. Rep. **449**, 3 (2007).
[16] G. T. Charras, T. J. Mitchison, and L. Mahadevan, J. Cell Sci. **122**, 3233 (2009).
[17] T. J. Mitchison, G. T. Charras, and L. Mahadevan, Semin. Cell Dev. Biol. **19**, 215 (2008).
[18] N. G. Cogan and R. D. Guy, HFSP J. **4**, 11 (2010).
[19] A. Tero, R. Kobayashi, and T. Nakagaki, Physica (Amsterdam) **205D**, 125 (2005).
[20] N. Okamura and S. Ishiwata, J. Muscle Res. Cell Motil. **9**, 111 (1988).
[21] F. Wottawah, S. Schinkinger, B. Lincoln, R. Ananthakrishnan, M. Romeyke, J. Guck, and J. Käs, Phys. Rev. Lett. **94**, 098103 (2005).
[22] H. Karcher, J. Lammerding, H. Huang, R. T. Lee, R. D. Kamm, and M. R. Kaazempur-Mofrad, Biophys. J. **85**, 3336 (2003).
[23] A. C. Callan Jones and F. Jülicher, New J. Phys. **13**, 093027 (2011).
[24] S. Günther and K. Kruse, New J. Phys. **9**, 417 (2007).
[25] A. Besser, J. Colombelli, E. H. K. Stelzer, and U. S. Schwarz, Phys. Rev. E **83**, 051902 (2011).
[26] S. Banerjee and M. C. Marchetti, Soft Matter **7**, 463 (2011).
[27] R. Peter, V. Schaller, F. Ziebert, and W. Zimmermann, New J. Phys. **10**, 035002 (2008).
[28] See Supplemental Material at http://link.aps.org/supplemental/10.1103/PhysRevLett.110.138102 for the model derivation in 2D.
[29] The boundary conditions are the nonflux condition for c and the Dirichlet condition for the w and u; $w(0) = 0$, $w(L) = 0$, $u(0) = 0$, and $u(L) = 0$.
[30] Darcy's law has the form $v = -\frac{\kappa}{\eta_f}\nabla p$. To obtain the drag force density, assume that $v = \text{const}$ and $u \equiv 0$ and compare this with Eqs. (4). Then, $\eta_f/\kappa = \beta\rho_s = \eta_f\rho_s/\kappa_0$ and the effective permeability $\kappa = \kappa_0/\rho_s$ depends on the solid volume fraction.
[31] R. Nagai, R. N. Yoshimoto, and N. Kamiya, J. Cell Sci. **33**, 205 (1978).
[32] S. Takagi and T. Ueda, Physica (Amsterdam) **237D**, 420 (2008).
[33] M. Radszuweit, H. Engel, and M. Bär, Eur. Phys. J. Special Topics **191**, 159 (2010).
[34] M. H. Köpf and L. Pismen, arXiv:1204.0402.